

High-precision sub-pixel interpolation in PIV/PTV image processing

by

H. Nobach, N. Damaschke and C. Tropea

Fachgebiet Strömungslehre und Aerodynamik
Technische Universität Darmstadt
Petersenstr. 30, 64289 Darmstadt, Germany

ABSTRACT

The main imaging processing task in a PIV/PTV measurement system is the derivation of a displacement vector from particle positions in two images taken in a particle-laden flow. Both, the particle-tracking velocimetry (PTV), which derives the displacement of individual particles, and the statistical particle image velocimetry (PIV) are potentially able to achieve a precision which is better than the nominal spatial resolution of the imaging system. In both cases, analysis methods must be used, which are able to precisely estimate the sub-pixel location of intensity peaks, either directly in the image for PTV or in the correlation plane for PIV. Furthermore, interpolation methods are required for the transform from image coordinates into real-world coordinates or for the estimation of velocity gradients, e.g. using a window deformation. Both, the interpolation and the estimation of the peak location have limited achievable accuracy due to a loss of information or due to a non-adequate model of the peak shape.

1. INTRODUCTION

The two techniques, particle image velocimetry (PIV) and particle tracking velocimetry (PTV) are analysing methods for image pairs taken in a seeded flow field with known temporal separation. The distance between the particle positions in the two images divided by the time separation yields the local velocity information. While the PTV method directly tracks single particles, the PIV method uses the cross-correlation function to derive the local motion statistically. Therefore, the possible accuracy of the PTV algorithm is given by the accuracy of the detection of particle positions, whereas the PIV method is limited by the accuracy of locating the correlation peak.

In both cases a transform from image coordinates into orthogonal real-world coordinates may also be necessary, e.g. for stereoscopic or any other non-orthogonal imaging. This requires a resampling of the images, as does also the window deformation technique [3, 12]. Since deviations of the interpolated intensity distribution directly influence the velocity estimate, this is a critical procedure, which should guarantee a minimum loss of information.

As no camera objective is ideal, the real particle images on the image plane are distorted due to the limited spatial bandwidth of the camera objective and due to aberrations. These two effects are combined in the point-spread function of the camera objective [11]. The investigations in section 2 show that the imaging model has a minor influence to the reachable accuracy and simplified models can be used.

In section 3 the loss of information due to the image interpolation is shown using different interpolation methods and an alternative method is introduced yielding better results.

Section 4 investigates the possible accuracy of displacement estimation between two images using the cross-correlation function between images.

In section 5 further influences are investigated and possible improvements of the algorithm are shown.

Section 7 introduces the test images and discusses the results.

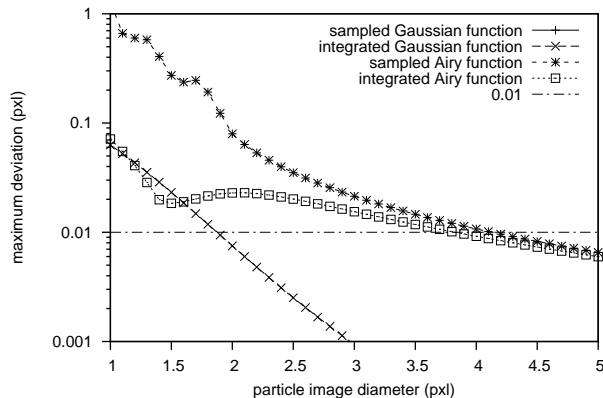


Figure 1: Maximum sub-pixel position bias for several intensity functions

Section 8 concludes with an outlook.

2. PARTICLE POSITION ESTIMATION

An accurate estimation of the particle position from the acquired images is essential for the PTV technique. A widely used method to derive the sub-pixel position of the intensity maximum is to fit a Gaussian function to the samples and to derive the maximum position of the interpolated function. Since the logarithm of a Gaussian function yields a second-order polynomial, the sub-pixel position δ of the interpolants maximum can be derived as

$$\delta = \frac{Y_{I-1} - Y_{I+1}}{2(Y_{I+1} - 2Y_I + Y_{I-1})} \quad (1)$$

relatively to the index I of the maximum sample, where Y_i is the logarithm of the function values y_i . This interpolation method works exactly for sampled Gaussian functions figure 1, the most simple model of the imaging process of small particles [14]. More complex imaging models as the intensity integration over the area of the photo sensors or the use of an Airy function as the imaging model have systematic errors due to the non-optimal sub-pixel interpolation method. However, for usual particle image diameters of 2...3 pxl the remaining bias of the position estimation is less than 0.1 pxl in all cases. To reduce this bias a more accurate model has to be fit to the available image data. Finding the correct model requires much information about the imaging system, which are not easily to obtain. On the other hand, the model fit often must be realized as an iterative optimization process, which is very costly. Furthermore, other bias sources have been found, which can be removed or at least reduced more easily. Therefore, the use of more complex sub-pixel interpolation methods for the particle position estimation is not used here. However, it could be implemented in the future.

3. IMAGE INTERPOLATION

Often in the PIV analysis, the image values are required at sub-pixel positions, e.g. the transformation of the coordinates of oblique images into real cartesian coordinates or the window deformation technique [3, 12]. Therefore, the image is interpolated using an interpolation function and resampled at new positions.

The image re-sampling is a crucial step for the appropriate reconstruction of the image signal as has been shown by [9]. In [12] several interpolation schemes have been mentioned. Higher-order polynomial functions are considered superior to the bi-linear interpolation, which is widely used due to its simplicity and robustness. Therefore, in addition to the bi-linear interpolation, a 3rd order polynomial interpolation, a Fourier series interpolation and a cardinal function interpolation [1] with a Hamming window to reduce the abruptness of the truncated ends of the sinc function [7] have been investigated.

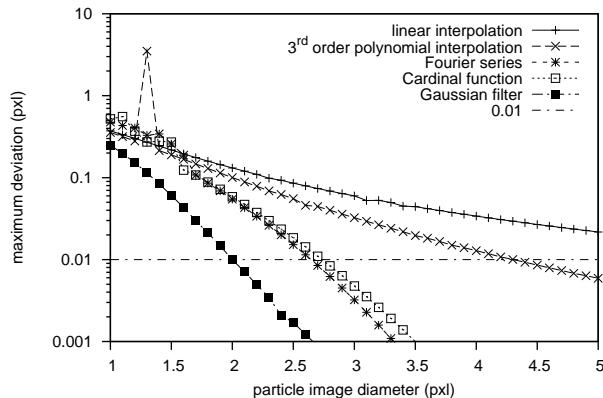


Figure 2: Maximum sub-pixel position bias after image interpolation for several interpolation methods

In figure 2 the maximum deviation of the sub-pixel position estimation is shown as a function of the width of the Gaussian function for several interpolation schemes. Indeed, the higher-order interpolation schemes are better than the simple linear interpolation. However, the remaining bias cannot be neglected. As mentioned in [12] the PIV signal spectrum has a major component in the high-frequency part, at least for diameters less than 3 pxl. The Nyquist criterion is not fulfilled and the particle images are under-sampled. Therefore, all interpolation schemes fail which use only the sampled function. Even the cardinal function has a significant bias of more than 0.01 pxl up to a particle image diameter of 2.7 pxl. This result is different from those in [10], which can be explained as a result of using larger particle images there.

More accurate results can be achieved using an optimized interpolation filter, recognizing the signal character and the signal model used for the estimation of the sub-pixel location. For high robustness a 11-point Gaussian filter is used with the coefficients

$$c_i(x) = \exp[-b(x-i)^2] \quad \text{for } i = X-5 \dots X+5 \quad (2)$$

where X is the rounded integer value of the resample positions $x = j + \delta_{res}$. The parameter b has been found to be optimal at $b = 0.5$ in terms of the achievable accuracy and the robustness in the presence of noise. The results in figure 2 show that this interpolation scheme is clearly superior to the other methods investigated. For a width of 2.1 pxl or more, a systematic error of less than 0.01 pxl remains.

The results of the Gaussian interpolation comply with [10], whereas the results using the sinc interpolation scheme do not. Obviously, the size of the particle image has been chosen there large enough to fulfil the Nyquist criterion sufficiently. On the other hand, the usual size of particle images is in the range of 2...3 pxl, where a significant bias remains for the sinc interpolation scheme, while the Gaussian interpolation scheme yields excellent results even in this range.

4. DISPLACEMENT ESTIMATION

In PIV analysis the displacement of a particle ensemble between two images is estimated using the cross-correlation function of the two images. To quantify the possible accuracy of the displacement estimation, two images are generated with single peaks but having different sub-pixel locations. From the maximum peak of the cross-correlation function the sub-pixel location of the peak is derived.

Figure 3 shows the results for two one-dimensionally sampled Gaussian functions with a peak width of 2.5 pxl. Even for this ideal case (single peak in each signal, sampled Gaussian function) a significant deviation can be seen between the estimated sub-pixel displacement and the simulation.

The cause of this phenomenon can be seen in figure 4. The continuous Gaussian function is sampled at discrete locations. Here the samples must fit the continuous function. Beside this, the autocorrelation function of the Gaussian function and the autocorrelation function of the sampled signal are shown. The autocorrelation function of the continuous Gaussian function is also a Gaussian function. A sub-

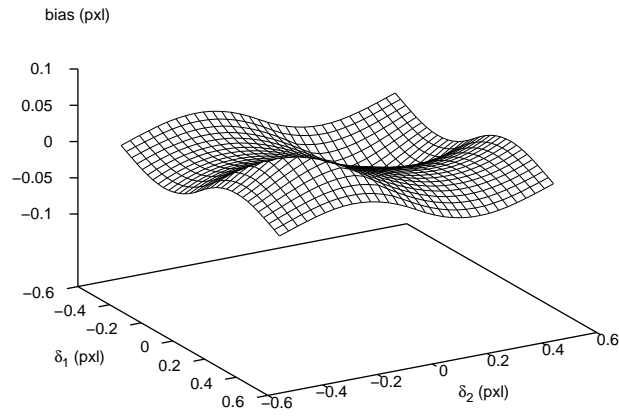


Figure 3: Sub-pixel displacement bias for two Gaussian intensity functions

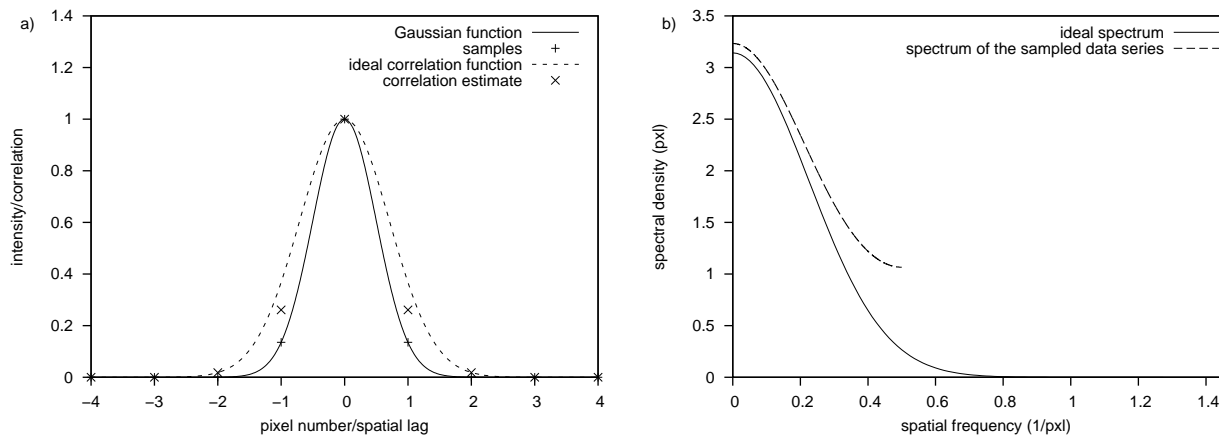


Figure 4: Deviation of the correlation estimate and the power spectral density function of the sampled series from the ideal Gaussian function

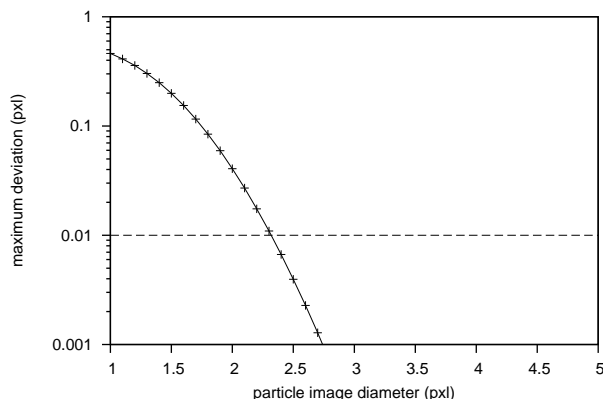


Figure 5: Maximum deviation of the displacement estimation

pixel location of a Gaussian correlation function could be accurately estimated. However, the discrete correlation function of the sampled function does not fit the continuous correlation function. Furthermore, even the shape is not Gaussian. The power spectral density of the Gaussian function has significant power in the frequency range above half the sampling frequency. Therefore, the Nyquist criterion is not fulfilled and a significant aliasing error can be seen. A bias remains in the sub-pixel estimation from the sampled correlation function even for a Gaussian signal.

In figure 5 the remaining bias of the sub-pixel displacement estimation from the correlation function is shown for a Gaussian intensity function as a function of the particle image width. Obviously, this influence limits the possible accuracy of the sub-pixel displacement estimation for small particle images. Note that the interpolation model and the simulation model are Gaussian, hence this bias cannot be avoided by better interpolation schemes. Two possible solutions to this problem are

- use of an appropriate interpolation scheme for the image data (see above) together with an over-sampling of the image. This yields a wider particle image (in pxl), which causes a smaller bias. On the other hand, this increases the computational costs. However, for one-step estimators this is the only solution,
- use of an iterative (multi-step) method with sub-pixel window shift (zero-displacement technique) [5, 6]. This also requires an accurate sub-pixel interpolation of the image data (see above). However, it iteratively optimizes the interrogation areas taken from the images so that there remains no displacement between the two interrogation areas and the sub-pixel interpolation yields no bias due to the symmetry.

5. FURTHER INFLUENCES AND IMPROVEMENTS

5.1 Gray-scale offset

An important bias source for the sub-pixel displacement is the non-zero background intensity. This directly causes an offset in the correlation function, which affects the shape of the peak. Two possible solutions are

- more complex imaging model, which includes an intensity offset. In that case the model fit becomes more complex and the parameter estimation must be realized as an iterative optimization process, which is very costly.
- use of an iterative (multi-step) method with sub-pixel window shift (zero-displacement technique) [5, 6], which optimizes the sub-pixel displacement between the interrogation areas to be zero.

The bias due to the gray offset is shown in figure 6, where a gaussian intensity function has been shifted by a constant value of 0.1 of the maximum intensity. A significant deviation can be seen, which decreases

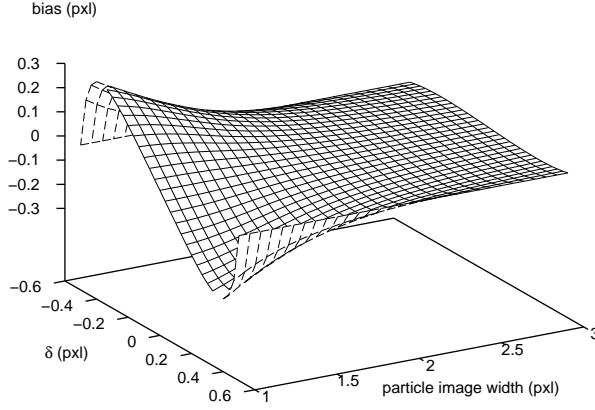


Figure 6: Sub-pixel position bias for a Gaussian intensity function with offset

for wider functions. For a width of 2 pxl this bias can reach 0.06 pxl and for a width of 3 pxl still more than 0.01 pxl.

5.2 Photon Noise

Due to the random character of the light and the imaging process, there is always a noise component in the images. The photon noise and the dark noise yield Poisson distributed gray values, which has an intensity dependent variance. The presumption of a Gaussian distributed noise yields a bias, which can be avoided using the square-root image instead of the obtained intensity image [4].

5.3 Particle Image Truncation

The use of interrogation windows for PIV analysis yields a sharp sub-division of the image. Due to the random distribution of particles in the observed area, particle images can occur close to the edge of the interrogation window leading to truncated particle images.

For the FFT-based correlation estimator a periodically continued function is assumed. For the two image intensity functions $z_1(i, j)$ and $z_2(i, j)$ this estimator can be written as

$$R(k, l) = \frac{1}{MN} \sum_{i=1}^M \sum_{j=1}^N z_1(i, j) z_2(i + k \bmod M, j + l \bmod M) \quad (3)$$

This estimator is strongly affected in the case of truncated particle images [8].

Alternative correlation estimators, as the direct correlation estimate, without presumed periodicity

$$R(k, l) = \frac{1}{MN} \sum_{i=\max(1, 1-k)}^{\min(M, M-k)} \sum_{j=\max(1, 1-l)}^{\min(N, N-l)} z_1(i, j) z_2(i + k, j + l) \quad (4)$$

or the normalized direct correlation estimate

$$R(k, l) = \frac{1}{(M - |k|)(N - |l|)} \sum_{i=\max(1, 1-k)}^{\min(M, M-k)} \sum_{j=\max(1, 1-l)}^{\min(N, N-l)} z_1(i, j) z_2(i + k, j + l) \quad (5)$$

do not significantly improve the situation.

The influence of the truncation error can be escaped with the alternative normalization using the variances of the two investigated image parts [14, 11], leading the correlation coefficient function

$$\rho(k, l) = \frac{\sum_{i=\max(1, 1-k)}^{\min(M, M-k)} \sum_{j=\max(1, 1-l)}^{\min(N, N-l)} z_1(i, j) z_2(i + k, j + l)}{\sqrt{AB}} \quad (6)$$

with

$$A = \sum_{i=\max(1,1-k)}^{\min(M,M-k)} \sum_{j=\max(1,1-l)}^{\min(N,N-l)} z_1^2(i, j) \quad (7)$$

$$B = \sum_{i=\max(1,1-k)}^{\min(M,M-k)} \sum_{j=\max(1,1-l)}^{\min(N,N-l)} z_2^2(i+k, j+l) \quad (8)$$

Even for truncated particle images this estimator yields the correct location of the maximum and significant smaller RMS values of the sub-pixel displacement estimation bias.

The use of an iterative (multi-step) method with sub-pixel window shift (zero-displacement technique) [5, 6], which optimizes the sub-pixel displacement between the interrogation areas to be zero is an alternative solution to avoid this influence. However, the combination of the normalization and the zero-displacement technique increases the convergence rate significantly.

5.4 Elliptical Particle Images

In [11] the problem of aberrations of the particle imaging in the image corners has been discussed. Here elliptical particle images can often be seen, which leads to a significant pixel locking effect if two one-dimensional sub-pixel displacement estimators are used for the two orthogonal velocity components. These authors introduced improved, two-dimensional estimators, which increase the computational costs significantly, due to their iterative character.

Even here, an iterative (multi-step) method with sub-pixel window shift (zero-displacement technique) [5, 6], which optimizes the sub-pixel displacement between the interrogation areas to be zero can be used to obtain bias-free sub-pixel displacement estimations.

6. THE ENTIRE PIV ESTIMATOR

The new estimator is an iterative (multi-step) method with sub-pixel window shift (zero-displacement technique) [5, 6]. The required re-sampling of the image data is realized using a Gaussian filter, which has been found to be superior to common interpolation schemes. The re-sampled images are cross-correlated using the normalization with the variances of the two investigated image parts [14, 11]. The interpolation of the correlation function to derive the sub-pixel location of the maximum peak is realized with the widely used polynomial interpolation to the logarithmic correlation values. To derive the two-dimensional maximum location two one-dimensional interpolations are used. To reduce the sensitivity of the sub-pixel displacement estimation to noise, the interpolation uses the four neighbours with 2pxl distance around the maximum value.

In figure 7 the final RMS value of the estimation is shown with and without photon noise. The quantisation noise has not been recognized here. A significant improvement can be seen for the new processing method (method 3) compared to conventional methods (methods 1 and 2). Furthermore, for particle images with a width of ≥ 1.7 pxl the RMS value is less than 0.01 pxl, which holds also for images with photon noise.

7. TEST IMAGES

A two-step algorithm with a full-pixel window shift (method 1) and a two-step algorithm with a sub-pixel window shift using a bi-linear interpolation (method 2) are compared to the new algorithm (method 3) using simulated and real images.

7.1 Simulated Images

The simulated images of $256 \text{ pxl} \times 256 \text{ pxl}$ consist of approximately 1000 particles, which have varying intensity and a particle image diameter of 3.0 pxl]. There is no velocity gradient. Figure 8 show the

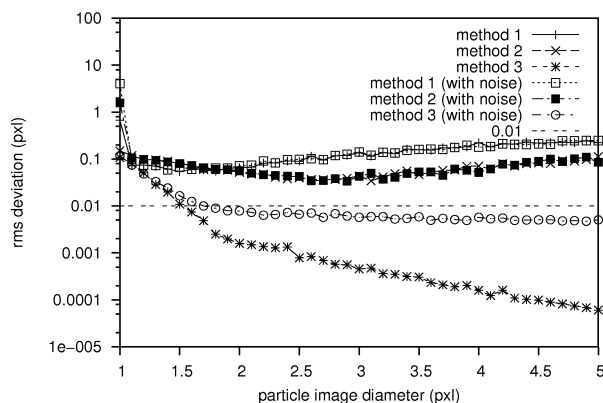


Figure 7: RMS value of the particle displacement estimation using a two-step algorithm with a full-pixel window shift (method 1), a two-step algorithm with a sub-pixel window shift using a bi-linear interpolation (method 2) and the multi-step algorithm with a sub-pixel window shift using a Gaussian interpolation filter (method 3)

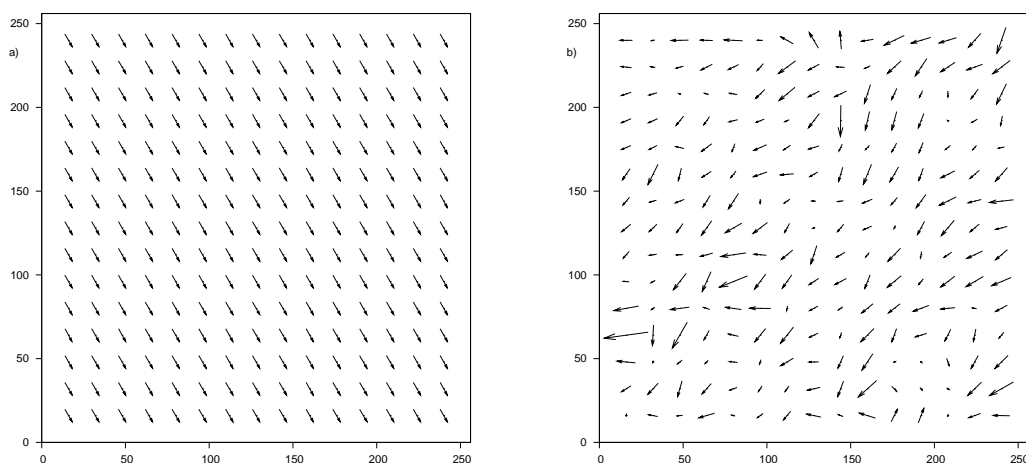


Figure 8: Two-step algorithm with a full-pixel window shift: (a) Obtained velocity vectors and (b) the deviation from the simulation.

obtained velocity vectors (a) and the deviation from the simulation (b) for the two-step algorithm with a full-pixel window shift (method 1). Figure 9 and figure 10 show the results for the two-step algorithm with a sub-pixel window shift using a bi-linear interpolation (method 2) and for the new algorithm (method 3) respectively.

While the velocity values are quite similar for all three estimation procedures, the deviations from the simulation have significant differences. Note that the drawn vectors are magified. The largest deviations can be seen for method 1 (full-pixel window shifts). Method 2 has reduced deviations. However, the bi-linear interpolation limits the achievable accuracy. Furthermore, the deviation vectors have a structure, which is a result of the truncated particle images. The new method (method 3) has significantly smaller deviations. Only at the image borders, the Gaussian filter runs out of data and the interpolation becomes unreliable.

7.2 Real Images

Real images always have the disadvantage, that the correct velocity values are not known. Furthermore, often velocity gradients occur. Therefore, only an example test can be shown here.

The test images used here are public domain images of a vortex from an experiment used for the PIV

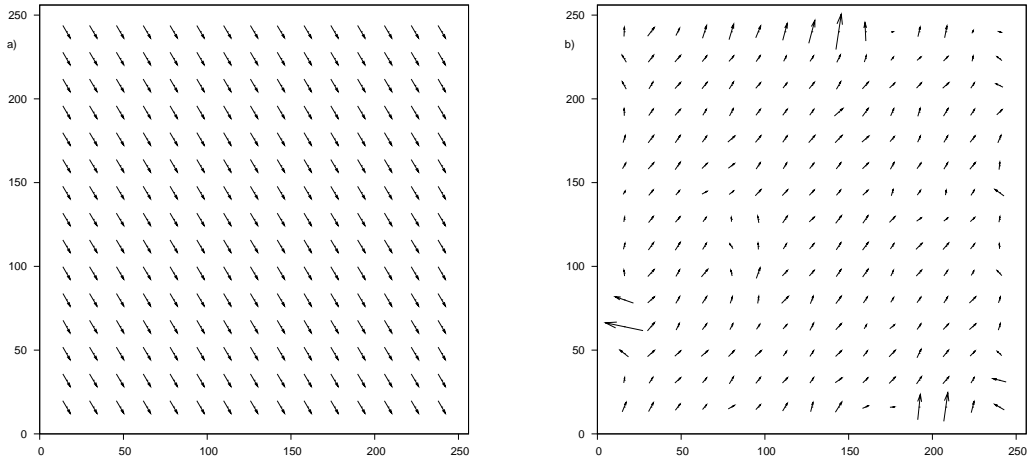


Figure 9: Two-step algorithm with a sub-pixel window shift using a bi-linear interpolation: (a) Obtained velocity vectors and (b) the deviation from the simulation.

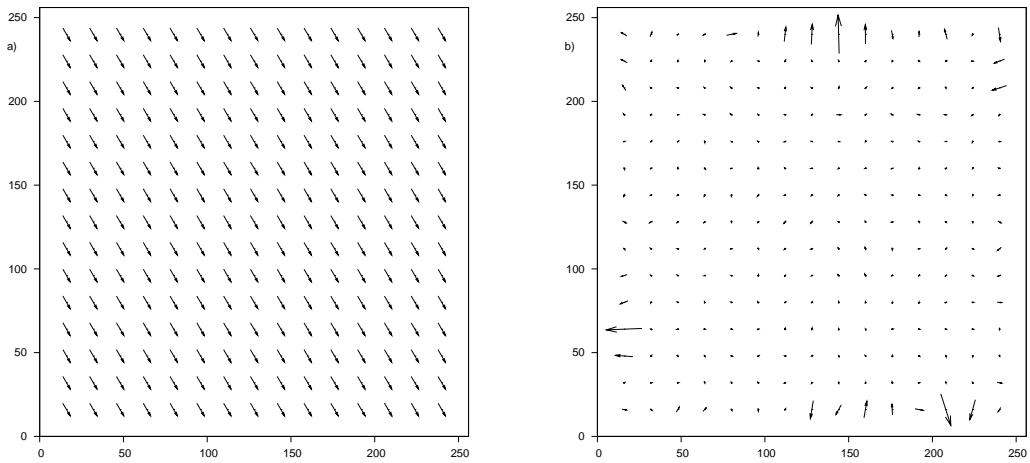


Figure 10: Multi-step algorithm with a sub-pixel window shift using a Gaussian interpolation filter: (a) Obtained velocity vectors and (b) the deviation from the simulation.

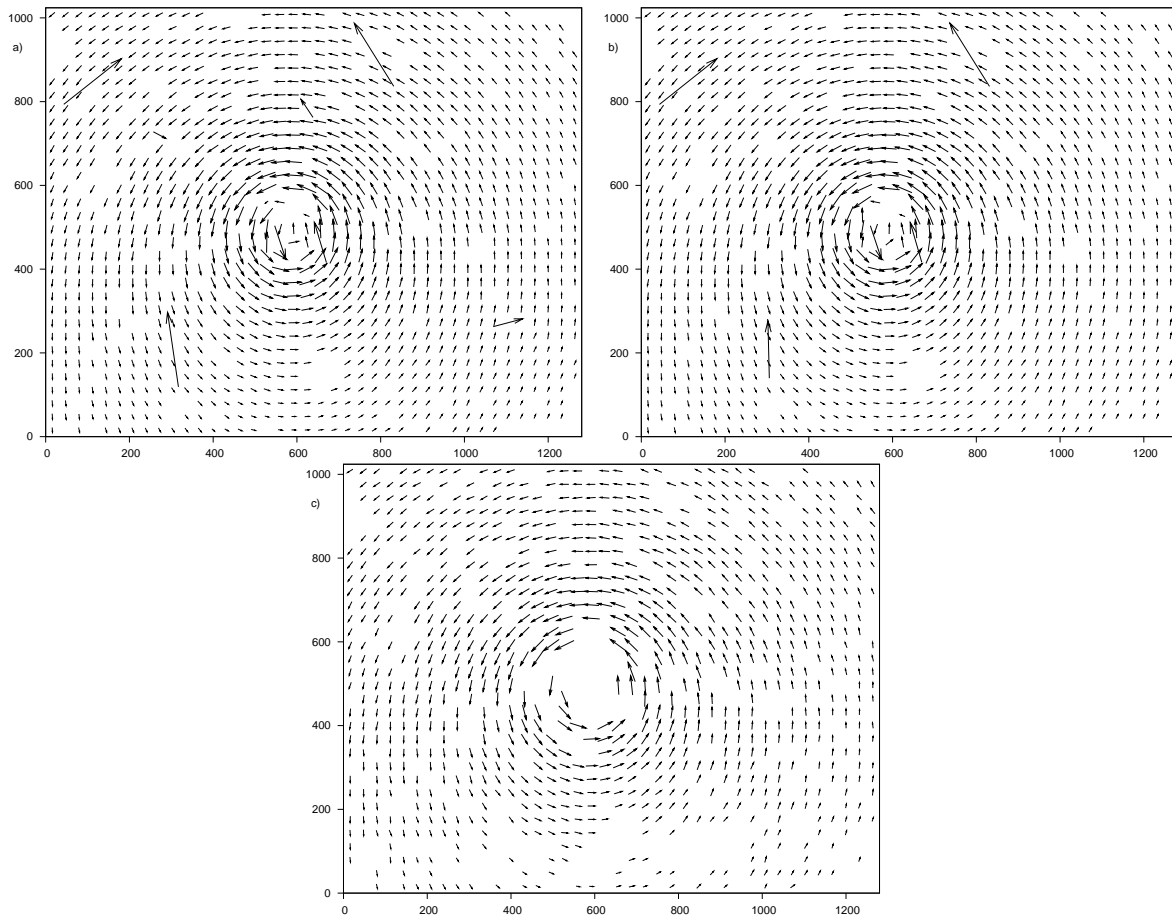


Figure 11: Results for real images: a) Two-step algorithm with a full-pixel window shift, b) Two-step algorithm with a sub-pixel window shift using a bi-linear interpolation and c) Multi-step algorithm with a sub-pixel window shift using a Gaussian interpolation filter.

Challenge 2001 [13].

Figure 11 shows the velocity vectors for the investigated estimation methods. The valid vectors of the three algorithms have no obvious difference. The higher accuracy, which is expected for the new method cannot be confirmed here, since no reference values are available. The two-step methods yield spurious vectors at some positions, while the new method reliably rejects the non-valid vectors. The iterative optimization algorithm does not converge in these cases, which can be used as an validation criterion. Therefore, the new algorithm is more reliable. The convergence as a built-in convergence criterion makes the algorithm more conservative. If the procedure converges, the result is expected to be more accurate. However, in the investigated test images strong gradients occur, which limits the achievable accuracy.

8. CONCLUSION

A new estimation procedure has been developed which yields high-precision displacement estimates. The fundamental improvement is the use of *a priori* information about the signal character to interpolate the image data. This interpolation scheme is superior to other interpolation schemes, like the commonly used bi-linear interpolation or higher-order polynomial interpolations. The new interpolator is even superior to the cardinal interpolation, which is often used as a reference. All these non-parametric interpolation schemes are limited by the fact that the particle images are strongly under-sampled and the Nyquist criterion is not fulfilled.

All other influences can be avoided using the iterative (multi-step) method with sub-pixel window shift (zero-displacement technique) [5, 6], which optimizes the sub-pixel displacement between the interrogation areas to be zero. Here the correlation peak is centered around zero, which yields bias free estimates, even if the function model is non-ideal.

The new algorithm reaches an accuracy of 0.01 pxl (RMS value) only if the investigated flow field is free of velocity gradients. In the case of gradients within the interrogation windows, the correlation peak is smeared. Furthermore, the irregular sampling of the image yields a displacement estimate which is locally weighted, hence the average is biased. In that case an improvement can be achieved by recognizing the velocity gradients during the correlation estimation [2].

ACKNOWLEDGEMENT

Funding from the Deutsche Forschungsgemeinschaft under grants Tr 194/21 is gratefully acknowledged.

REFERENCES

- [1] E L Hall. *Computer Image Processing and Recognition*. Academic, New York, 1979.
- [2] D P Hart. Piv processing using multidimensional correlation. In *Proc. 10th Int. Symp. on Flow Visualization*, Kyoto, Japan, 2002. paper F0374.
- [3] H T Huang, H E Fiedler, and J J Wang. Limitation and improvement of piv; part ii: Particle image distortion, a novel technique. *Exp. in Fluids*, 15:263–273, 1993.
- [4] B Jähne. *Practical Handbook on Image Processing for Scientific and Technical Applications*. CRC Press, Boca Raton, 2 edition, 2003.
- [5] C J Kähler. Multiplane stereo piv — recording and evaluation methods. In *Proc. Euromech 411*, Rouen, France, 2000.
- [6] B Lecordier, J C Lecordier, and M Trinité. Iterative sub-pixel algorithm for the cross-correlation piv measurements. In *Proc. 3rd Int. Workshop on PIV*, University of California, Santa Barbara, USA, 1999.
- [7] W Niblack. *An Introduction to Digital Image Processing*. Prentice-Hall, Englewood Cliffs, NJ, 1986.
- [8] J Nogueira, A Lecuona, and P A Rodriguez. New source of peak locking to the window size: analysis and its removal. In *Proc. 4rd Int. Workshop on PIV '01*, Göttingen, Germany, 2001. paper 1013.
- [9] W K Pratt. *Digital image Processing*. Wiley, New York, 1978.
- [10] T Roesgen. Optimal subpixel interpolation in particle image velocimetry. *Exp. in Fluids*, 35:252–256, 2003.
- [11] O Ronneberger, M Raffel, and J Kompenhans. Advanced evaluation algorithms for standard and dual plane particle image velocimetry. In *Proc. 9th Int. Symp. on Appl. of Laser Techn. to Fluid Mechanics*, Lisbon, Portugal, 1998. paper 10.1.
- [12] F Scarano. Iterative image deformation methods in piv. *Meas. Sci. Technol.*, 13:R1–R19, 2002.
- [13] M Stanislas, K Okamoto, and C Kähler. Main results of the first international piv challenge. *Meas. Sci. Technol.*, 14(10):R63–R89, 2003.
- [14] C E Willert and M Gharib. Digital particle image velocimetry. *Exp. in Fluids*, 10:181–193, 1991.